MOLECULAR AND CELLULAR BIOLOGY, July 2005, p. 5599–5606 Vol. 25, No. 13
0270-7306/05/$08.00+0 doi:10.1128/MCB.25.13.5599–5606.2005

Mice with a Disruption of the Thrombospondin 3 Gene Differ in Geometric and Biomechanical Properties of Bone and Have Accelerated Development of the Femoral Head

Kurt D. Hankenson,[1]† Sheriar G. Hormuzdi,[2]†‡ Jeffrey A. Meganck,[3] and Paul Bornstein[2,4]*

Departments of Orthopaedic Surgery, and Cell and Developmental Biology and Unit for Laboratory Animal Medicine[1] and Mechanical Engineering,[3] University of Michigan, Ann Arbor, Michigan 48109, and Departments of Biochemistry[2] and Medicine,[4] University of Washington, Seattle, Washington 98195

Received 6 January 2005/Returned for modification 4 March 2005/Accepted 27 March 2005

Thrombospondin 3 (TSP3) is structurally similar to cartilage oligomeric matrix protein (COMP/TSP5), but its function is unknown. To determine the functional significance of TSP3, we generated mice with a targeted disruption of *Thbs3*. TSP3-null mice are viable and fertile and show normal prenatal skeletal patterning, based on Alcian blue/Alizarin red S staining. However, subtle and transient abnormalities were detected in the developing postnatal skeleton. Young adult TSP3-null mice are heavier than controls, and analyses of the geometric and biomechanical properties of long bones show increases in the moments of inertia, endocortical and periostal radii, and failure load. The bones of 9-week-old TSP3-null male mice also have a significantly greater cortical area. Most of these differences were no longer detected in 15-week-old mice. Microcomputed tomography scans showed that the trabecular bone proximal to the femoral head growth plate developed at an earlier time in TSP3-null mice than in wild-type mice. Thus, vascular invasion and ossification start in the femoral heads of TSP3-null mice at 9 weeks, whereas the wild-type femoral head is still composed of hypertrophic chondroctyes in a calcified matrix at 15 weeks. These results provide evidence for a role for TSP3 in the regulation of skeletal maturation in mice.

Thrombospondin 3 (TSP3; encoded by *Thbs3*) was first discovered during sequencing of DNA upstream from the start of transcription of the mouse *Muc1* (episialin) gene (31). Subsequent studies showed that these two genes are part of a tightly organized, conserved gene cluster on chromosome 3, E3-F1, which also includes glucocerebrosidase (*Gba*) and metaxin 1 (*mtx1*). The latter two genes are transcribed divergently and share a common promoter region of about 1 kb (5, 9, 32). However, despite this genomic arrangement, and the presence of an enhancer of TSP3 in intron 6 of the metaxin gene (10), no metabolic interactions have been identified among any of the products of these four genes.

The TSP family consists of five members and can be divided into two groups. TSP1 and TSP2 are trimers with a chain molecular mass of 145 kDa, whereas TSPs 3 to 5 are pentamers with a subunit mass of ≈110 kDa. TSPs 3 to 5 differ from TSPs 1 and 2 in that they lack the procollagen domain and type I repeats of the trimeric proteins and contain four rather than three type II (epidermal growth factor-like) repeats (1, 6).

The expression of TSP3 mRNA has been studied in the developing mouse (17, 25), chicken (28), *Xenopus laevis* (30), and adult human tissues (2). Expression was detected in the perichondrium and in the proliferating zone of the growth plate in long bones and vertebrae after day 15, in the dentate gyrus, accessory olfactory bulbs, hippocampus, and choroid plexus of the brain after day 17, and in the terminal bronchi and alveoli of the lung after day 17. Qabar et al. (26), using midline sagittal sections of whole embryos, reported expression in the forming musculature of the body wall and intestine, in the sternum and vertebrae, and in the brain and lung. Qabar et al. (25) also identified TSP3 protein by immunohistochemistry with an antipeptide antibody in extraembryonic membranes, developing cartilage, several tissues of the eye, dorsal root ganglia, peripheral nerve, and brain of mouse embryos. However, the specificity of the antibody that was used in this study is questionable, since in another study it stained all tissues in some sections indiscriminantly (26). In the chicken, TSP3 mRNA was expressed in embryonic cartilage and in neurons that are actively extending processes (28), and in *Xenopus* embryos TSP3 mRNA was detected in the notocord, floor plate, sensorial layer of the ectoderm, and sensory epithelia (30).

Pentameric TSPs, including TSP3, form α-helical coiled-coil domains in which the axial channel or pore is lined by hydrophobic amino acids (12, 22, 24). In the case of TSP5/COMP this axial pore is capable of binding physiologically relevant hydrophobic molecules such as vitamin D and all-*trans* retinol with appropriate affinities (14), and this property is likely to extend to TSP3. More recently, the crystal structure of TSP5/COMP complexed with vitamin D_3 has been solved and shows the presence of two D_3 molecules arranged head-to-head in the channel (23). Despite these studies and information con-

* Corresponding author. Mailing address: Department of Biochemistry, Box 357350, University of Washington, Seattle, WA 98195. Phone: 206-543-1789. Fax: 206-685-4426. E-mail:bornsten@u.washington.edu.

† These two authors contributed equally.

‡ Present address: University Hospital of Neurology, Heidelberg, Germany.

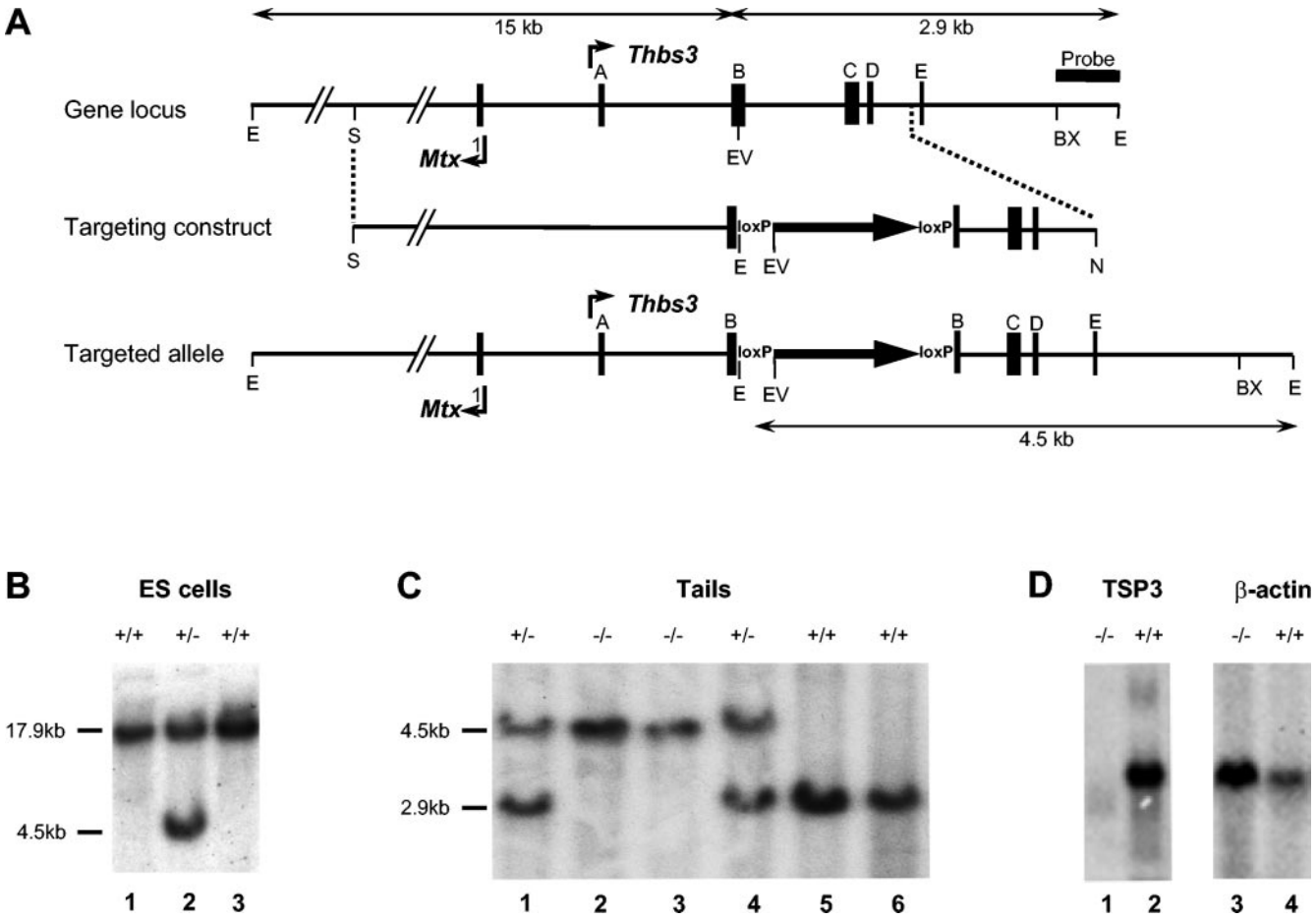

FIG. 1. Map of the murine wild-type and mutant Thbs3 loci and of the targeting construct used to generate the mutant Thbs3 gene. (A) A 17.9-kb fragment of the wild-type locus and its derivatives in the targeting construct and targeted allele are shown. Positions of the transcriptional start sites of the *Thbs3* gene, within exon A, and of the *Mtx1* gene, within exon 1, are indicated. Exons B, C, D, and E of the *Thbs3* gene, the BstXI-EcoRI fragment, which served as a probe for Southern analysis, the position of the *loxP* sequences flanking the PGK-neomycin gene (large arrow) within exon B, and the sizes of the restriction fragments, which were generated in the genotyping of ES cells and mice, are also shown. The locations of the restriction enzyme sites for BstXI (BX), EcoRI (E), EcoRV (EV), SalI (S), and NotI (N) are indicated. The NotI site is derived from the vector that was used to clone the targeting construct. The 3′ terminus of the homologous TSP3 genomic sequence in the targeting construct is known to be located in intron D (dotted line) but the precise location has not been determined. (B) Genotyping of targeted ES cell clones by Southern blot analysis. A representative blot shows EcoRI-restricted fragments diagnostic for wild-type (lanes 1 and 3) and targeted (lane 2) ES cell clones. (C) A representative Southern blot shows EcoRI- and EcoRV-restricted fragments diagnostic for wild-type (lanes 5 and 6), heterozygous (lanes 1 and 4), and homozygous mutant (lanes 2 and 3) mice. (D) Northern blot analysis of RNA extracted from lung tissue of wild-type (lanes 2 and 4) and *Thbs3* knockout mice (lanes 1 and 3). RNA was separated on a 1.2% agarose gel, and hybridized with a *Thbs3* probe (lanes 1 and 2), and after stripping the blot, with a β-actin probe (lanes 3 and 4).

cerning the spatial and temporal expression of TSP3, there is presently no good indication of the function of the protein in vivo. Accordingly, we performed a targeted disruption of the *Thbs3* gene in mice. Interestingly, despite normal skeletal patterning in utero, TSP3-null mice have an altered pattern of postnatal bone modeling. While wild-type and TSP3-null mice have similar bone mass, TSP3-null bone is geometrically distributed farther from a central axis, resulting in enhanced mechanical function. TSP3-null mice also have altered endochondral bone formation, with accelerated ossification of the femoral head.

MATERIALS AND METHODS

Generation of mutant mice. A mouse 129 genomic EcoRI subclone containing a 17.9-kb region of the *Thbs3*/*Mtx1* locus, including exons A, B, C, and D of the *Thbs3* gene and the entire divergently transcribed metaxin1 (*Mtx1*) gene, was used to generate the targeting construct. This sequence, the targeting construct, and the targeted allele derived from it are shown schematically in Fig. 1. In the targeting construct, a neomycin phosphotransferase gene, under the control of the phosphoglycerate kinase I promoter (PGK-Neo) and flanked by *loxP* elements, was inserted at the EcoRV restriction endonuclease cleavage site in exon B. These steps resulted in the insertion of an in-frame stop codon and the introduction of EcoRI and EcoRV restriction sites upstream from the PGK-Neo cassette.

RW4 embryonic stem (ES) cells (129SvJ; Genome Systems) were cultured on neomycin-resistant fibroblasts in high-glucose Dulbecco's modified Eagle's medium supplemented with 15% fetal calf serum (ES-qualified; Gibco-BRL), 0.1 mM β-mercaptoethanol, 2 mM L-glutamine, 100 U/ml penicillin G, 100 μg/ml streptomycin, nonessential amino acids (0.1 mM each; Gibco-BRL), and 1,000 units/ml of leukemia inhibitory factor (Gibco-BRL). Cells (2×10^7) were electroporated with 30 μg of targeting DNA and linearized by digestion with SalI. Selection with G418 was started 24 h after electroporation, and resistant clones were picked 8 to 10 days later. Identification of ES cells containing correctly

targeted clones was performed by Southern blot analysis. DNA was extracted as described by Laird et al. (20), digested with EcoRI, and analyzed by Southern blotting. The ≈600-bp BstXI-EcoRI genomic probe was located 3′ to the *Thbs3* sequence present in the targeting vector (Fig. 1) and detected 17.9- and 4.5-kb fragments derived from the wild-type and targeted alleles, respectively (Fig. 1B).

To avoid poor germ line transmission due to karyotypic abnormalities in ES cells (21), we determined the karyotypes of correctly targeted clones and selected those with a normal complement of chromosomes for blastocyst injection. Chimeric mice generated from successfully injected blastocysts were bred to produce homozygous *Thbs3*$^{-/-}$ mice. Southern blot analysis of tail DNA, restricted with EcoRI and EcoRV and hybridized with the BstXI-EcoRI genomic probe, was used to determine the genotype of mice. This procedure detected the 2.9- and 4.5-kb fragments derived from the wild-type and mutant alleles, respectively (Fig. 1C).

Northern blot analysis. RNA extracted from the lungs of 40-day-old wild-type and TSP3$^{-/-}$ littermates by the guanidium thiocyanate method (8) was subjected to Northern blot analysis. RNA was separated on a 1.2% agarose gel containing 2.2 M formaldehyde and, after transfer to Zetabind membrane (Cuno Inc., Meriden, CT), was hybridized with a 1.1-kb ^{32}P-labeled *Thbs3* cDNA probe that extended from the start of translation to an XhoI site in the type II repeats (4). The same blot was also probed with a mouse β-actin fragment obtained from Ambion Inc.

Histological analysis. Sections of lung, liver, kidney, stomach, small and large intestine, cerebrum, cerebellum, long bone (femur and tibia), pancreas, spleen, heart, thymus, colon, and spine were fixed in 10% formalin and embedded in paraffin. Sections were stained with hematoxylin and eosin and examined by light microscopy.

Skeletal development. To examine primary skeletal growth and development in utero, eight wild-type and seven TSP2-null embryos were harvested from two wild-type and TSP3-null females, respectively, at day 18 postcoitus. The embryos were fixed in 70% ethanol and stained with Alizarin red S and Alcian blue. To examine postnatal skeletal development, femurs were harvested from both male and female TSP3-null and wild-type mice at 9 and 15 weeks. Femurs to be used for microcomputed tomography and four-point bending studies were stored in phosphate-buffered saline at 4°C prior to testing. Femurs to be used for histological analysis were stored in 10% neutral buffered formalin at 4°C. Histological analysis was performed on TSP3-null specimens at each time point by decalcifying specimens, embedding in paraffin, sectioning with a microtome, and staining with hematoxylin and eosin or Safranin-O. In some cases, femurs were left undecalcified and embedded in plastic, thin sectioned and stained using von Kossa's method or toluidene blue.

Skeletal geometry. Geometrical properties of the harvested femurs were determined using microcomputed tomography (microCT). Femurs were scanned at 18-μm voxel resolution (GE Medical Systems) using the Parker method, and three-dimensional images were reconstructed. Diaphyseal bone length was measured directly on the resulting reconstructed image from the lesser trochanter to the most proximal point of the distal epiphyseal growth plate. These images were then thresholded using a previously defined method (19). The midcortical geometrical properties were determined in a 3-mm segment of the middiaphysis using custom software. The center plane of this 3-mm segment was defined as the midpoint between the most lateral point of the lesser trochanter and the most proximal point of the distal epiphyseal growth plate (15). The geometrical properties that were analyzed were cross-sectional area, cortical thickness, moment of inertia, and endocortical and periosteal radii. The endocortical radius extends from the centroid of the section to the endocortical surface and the periosteal radius is defined as the distance from the centroid to the periosteal surface. Trabecular bone parameters in a 1-mm^3 region proximal to the distal femoral growth plate were evaluated utilizing the stereology function of GE Medical Systems Microview software.

To assess femoral head development, coronal planes from three-dimensional images of each specimen were grouped into one of three categories: homogenous gray density without trabeculation, partial trabeculation, or fully trabeculated femoral head, with an absence of the growth plate. All subjective analyses were preformed by two blinded, independent viewers.

Mechanical testing of femurs. Femurs were loaded to failure in four-point bending at 0.5 mm/s in the anterior-posterior direction using a servohydraulic testing machine (810 Material Test System; Eden Prairie, MN). Regions loaded in four-point bending corresponded to those measured by microCT, where the anterior surface was in compression and the posterior surface was in tension. Crosshead displacement was monitored using an external linear variable displacement transducer (Lucas Control Systems; Hampton, VA) and load data were collected with a 50 lb load cell (Sensotec; Columbus, OH). Load-displacement curves were analyzed for whole bone stiffness, yield load, failure load, yield displacement, and failure displacement.

Statistical analysis. Results were analyzed for statistical significance within an age and gender group using two-tailed Student's *t* test, assuming equal variance. Results were considered to be statistically significant if P is <0.05.

RESULTS

Generation of *Thbs3*-null mice. Targeted ES cell clones were generated by homologous recombination of the targeting vector sequence shown in Fig. 1A and selected by resistance to G418. Southern analysis of EcoRI-restricted DNA from these clones, hybridized with a genomic fragment that was 3′ to the sequence in the targeting vector, identified a correctly targeted clone (Fig. 1B, lane 2). This result was confirmed by Southern analysis with a fragment that was 5′ to the targeting vector, but within the 17.9-kb EcoRI genomic DNA fragment. In correctly targeted clones, this probe identified the 15-kb fragment derived from the disrupted allele (data not shown). ES cell clone 239, which was karyotypically normal, was injected into blastocysts, and the blastocysts were transplanted into the uterine horns of pseudopregnant females. Several high-percentage chimeras were bred with C57BL/6 and 129SvJ mice to generate homozygous mutant mice. Genotyping of these mice by Southern analysis of tail DNA, restricted with EcoRI and EcoRV, showed the presence of only a 4.5-kb fragment (Fig. 1C, lanes 2 and 3). Heterozygous mice contained the mutant allele-derived 4.5-kb and the wild-type allele-derived 2.9-kb fragments (Fig. 1C, lanes 1 and 4), whereas wild-type mice contained only the 2.9-kb fragment (Fig. 1C, lanes 5 and 6).

Southern analysis of genomic DNA in ES cells and mice clearly documented the insertion of the neomycin gene in the mutant *Thbs3* allele (Fig. 1B and C). This insertion introduces an in-frame stop codon 5′ to the first loxP element and is expected to create a null *Thbs3* allele. This prediction was supported by Northern analysis of RNA isolated from lungs of homozygous mutant mice and their wild-type litter mates (Fig. 1D). Whereas abundant transcript was detected in the lungs of wild-type mice (Fig. 1D, lane 2), the lungs of homozygous mutant mice lacked detectable *Thbs3* transcript (Fig. 1D, lane1). A similar result was obtained by Northern analysis of RNA derived from brain (data not shown).

Characterization of TSP3-null mice. Physical examination of homozygous mutant mice indicated that there were no obvious anatomical differences from their wild-type littermates. *Thbs3*-null mice developed normally and were fertile. An extensive histological examination was undertaken to determine whether tissue structure was also normal at the light microscopic level. Accordingly, microscopic evaluation of many adult tissues was conducted, including those that had been shown previously to express significant amounts of TSP3 mRNA or protein, e.g., lung, cartilage, brain and small intestine. However, these studies failed to reveal significant abnormalities in *Thbs3*-null mice (results not shown).

Skeletal development. Alcian blue and Alizarin red S staining was used to evaluate distribution of cartilage and bone in day 18 whole embryos. There was no notable difference in skeletal patterning between TSP3-null and wild-type mice (data not shown). Interestingly, both male (22.3 versus 24.7 g) and female (18.7 versus 20.2 g) TSP3-null mice were signifi-

TABLE 1. TSP3-null femurs show increased periosteal diameters and greater moments of inertia[a]

Gender	Age (wk)	Genotype	Sample no.	Moment of inertia (mm^4)	Cortical thickness (mm)	Periosteal diam (mm)	Endocortical diam (mm)	Cortical area (mm^2)
Female	9	Wild type	7	0.09 ± 0.01	0.20 ± 0.01	0.56 ± 0.01	0.37 ± 0.005	0.72 ± 0.04
		Null	9	0.12 ± 0.01*	0.19 ± 0.005	0.64 ± 0.01*	0.46 ± 0.02*	0.77 ± 0.004
	15	Wild type	8	0.11 ± 0.01	0.22 ± 0.01	0.58 ± 0.01	0.38 ± 0.01	0.78 ± 0.02
		Null	7	0.14 ± 0.004	0.23 ± 0.01	0.64 ± 0.01	0.43 ± 0.01	0.89 ± 0.02
Male	9	Wild type	13	0.11 ± 0.01	0.20 ± 0.004	0.59 ± 0.01	0.40 ± 0.01	0.77 ± 0.03
		Null	6	0.16 ± 0.01*	0.22 ± 0.01	0.67 ± 0.01*	0.48 ± 0.00*	0.91 ± 0.05*
	15	Wild type	6	0.14 ± 0.01	0.24 ± 0.01	0.62 ± 0.02	0.40 ± 0.01	0.94 ± 0.03
		Null	7	0.18 ± 0.01*	0.23 ± 0.01	0.68 ± 0.004*	0.48 ± 0.01*	0.98 ± 0.05

[a] Values represent the mean ± SEM. *, $P < 0.05$.

cantly heavier at 9 week, but this difference was no longer apparent at 15 week.

To assess postnatal skeletal development in more detail, we harvested femurs from wild-type and TSP3-null mice at various ages and from both genders. Mid-cortical femoral geometric analyses were performed, and distal femoral trabecular bone was evaluated by microCT, as previously described (15). Moments of inertia were significantly higher for TSP3-null mice in comparison to wild-type mice for males at both 9 and 15 weeks and for females at 9 weeks of age (Table 1.). The moment of inertia quantifies geometrical distribution of bone about a central axis, so an increase can be related to either thicker bone (cortical thickness) or an equivalent thickness of bone located further from the central axis. TSP3-null mice did not show an increase in cortical thickness, but had greater periosteal and endocortical diameters in comparison to the wild-type mice for males at 9 and 15 weeks and for female mice at 9 weeks of age (Table 1). In older male mice these measurements also reverted to normal (data not shown). Additionally, the 9-week-old TSP3-null male mice had an increase in cortical area. Upon analysis of the distal femurs, there were no differences in trabecular bone volume fraction (data not shown).

The midfemoral results indicate that the marrow cavity is increased in volume in TSP3-null mice and that equivalent bone content is located farther from the central bone axis. To determine if these differences in bone geometry resulted in a difference in mechanical function, a four-point bending analysis was performed (Table 2). Failure loads were higher for both male and female TSP3-null mice than for their wild-type counterparts at 9 weeks of age, and at 9 weeks male TSP3-null mice also had a greater stiffness and yield load (Table 2). These differences were not apparent at 15 weeks.

TABLE 2. TSP3-null femurs show increased bending strength[a]

Gender	Age (wk)	Genotype	Sample no.	Stiffness (N/mm)	Yield load (N)	Failure load (N)
Female	9	Wild type	7	207.3 ± 16.6	18.2 ± 2.1	26.0 ± 2.7
		Null	9	233.8 ± 13.3	20.5 ± 1.2	33.2 ± 1.5*
	15	Wild type	8	242.0 ± 7.2	23.2 ± 2.2	31.1 ± 1.5
		Null	7	342.5 ± 17.9	25.8 ± 1.3	40.4 ± 1.5
Male	9	Wild type	13	203.6 ± 10.0	18.6 ± 1.0	25.8 ± 1.4
		Null	6	272.7 ± 21.2*	22.7 ± 1.3*	36.1 ± 1.4*
	15	Wild type	6	316.3 ± 29.0	28.0 ± 2.9	40.1 ± 2.9
		Null	7	310.1 ± 9.9	29.6 ± 2.6	46.5 ± 2.6

[a] Values represent the mean ± SEM. *, $P < 0.05$.

Ossification of the femoral head. While analyzing microCT scans of the midfemur we noticed a pronounced difference in morphology of TSP3-null femoral heads, relative to the wild type. At 9 and 15 weeks, TSP3-null mice showed a trabecular bone pattern in the proximal femoral head, whereas those from wild-type mice showed a homogenous gray area throughout the entire epiphysis of the femoral head, proximal to the growth plate (Fig. 2). To evaluate these differences in a more rigorous manner, microCT scans of the femoral head were analyzed by two blinded observers and scored according to one of three criteria: no trabeculation, partial trabeculation, or complete trabeculation (Table 3). The two observers were in complete agreement. At both 9 and 15 weeks there was no trabeculation of the wild-type femoral head. However, at 9 weeks, greater than 50% of TSP3-null bones showed partial trabeculation; by 15 weeks 100% of the male and 33% of the female TSP3-null femoral heads were completely trabeculated, and the remainder of the female femoral heads were partially trabeculated.

To examine this difference in femoral head morphology at the cellular level, decalcified paraffin-embedded sections were examined by histology. Surprisingly, the homogenous gray densities on microCT corresponded to areas of hypertrophic chondroctyes (Fig. 3A, C, and E), whereas trabeculated areas on microCT were clearly areas of active ossification (Fig. 3B, D, and F).

It is important to note that growth plate cartilage and articular cartilage typically are radiolucent on microCT, but histological analysis revealed that the homogenous gray areas on microCT were also hypertrophic chondroctyes (Fig. 3). Given that gray-white densities on microCT correspond to mineralization, we postulated that this region was composed of calcified cartilage. To determine whether the gray densities on microCT indeed corresponded to calcified cartilage, we examined undecalcified thin sections through the femoral head of wild-type mice. Von Kossa staining confirmed that this area was indeed calcified cartilage (results not shown). Thus, the femoral head of wild-type mice is still composed of calcified cartilage at 15 weeks, while that of the TSP3-null has begun to ossify, and in the case of male mice, there is no remaining calcified cartilage and the process of trabeculation has been completed.

DISCUSSION

The skeletal phenotype of TSP3-null mice is complex and includes transient geometric and biomechanical changes in

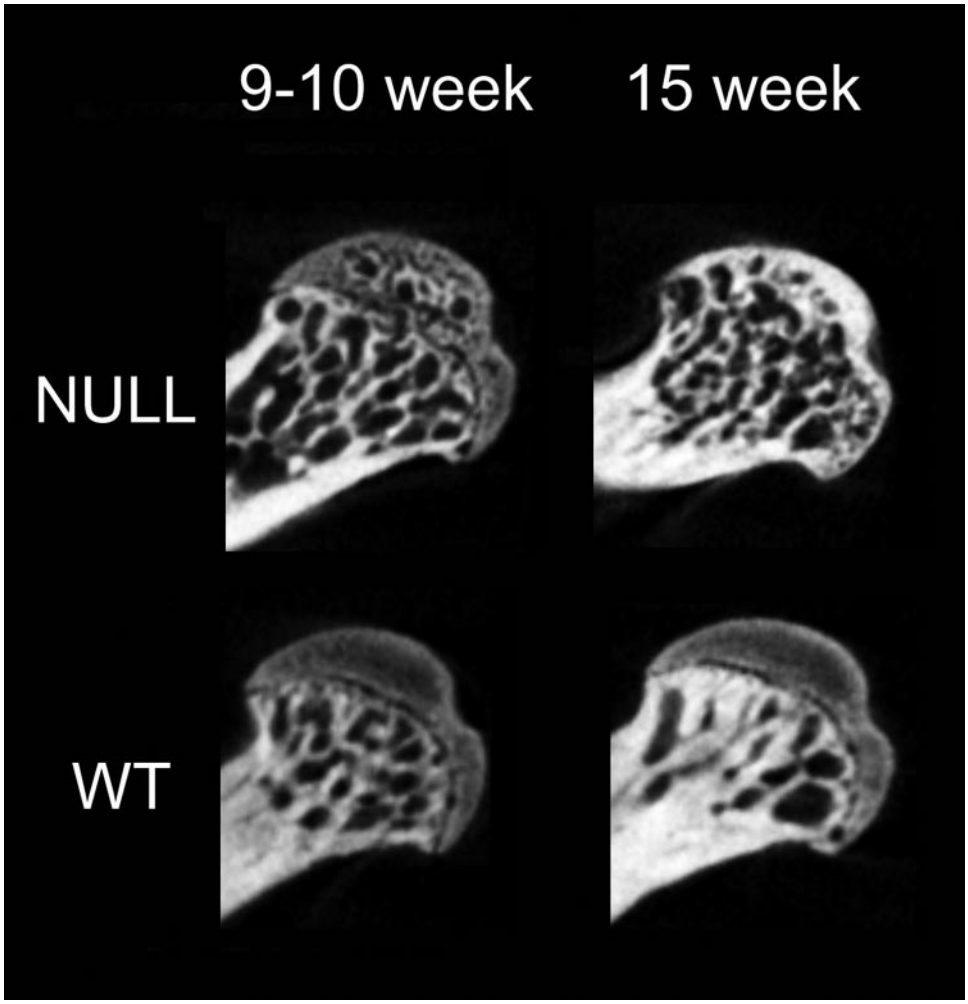

FIG. 2. TSP3-null mice show accelerated femoral head ossification. Representative microCT slices show the pattern of trabeculation in the femoral heads of TSP3-null and wild-type male mice at 9 and 15 weeks. Trabecular bone is already apparent in TSP3-null mice proximal to the femoral head growth plate at 9 weeks, and trabeculation is almost totally complete by 15 weeks. Note the homogenous gray area in the femoral head of wild-type mice proximal to the growth plate, which corresponds to hypertrophic chondrocytes. The resolution of these single-plane images is 18 μm/pixel. The differences in femoral head morphology can best be appreciated by comparing single-plane scans.

long bones and premature formation of trabecular bone proximal to the growth plate of the femoral head. Since TSP3 is expressed by both osteoblasts and chondrocytes, changes in bone structure and function are not unexpected. The geometric changes in femoral midcortical bone may reflect the fact that TSP3-null mice are skeletally more mature than their wild-type counterparts. Brodt et al. (7) have examined the effect of age on the femoral properties of C57BL/6 mice and found that moments of inertia, endocortical and periosteal diameter, and bending rigidity (stiffness) increased with age. Accelerated maturation of bone in TSP3-null mice is also suggested by the enhanced rate of endochondral ossification in the cartilage of the femoral head. In wild-type mice the femoral head does not undergo complete ossification for several months postnatally (29), but TSP3-null mice showed a very clear acceleration in the rate of femoral head endochondral ossification.

TABLE 3. TSP3-null femoral heads ossify earlier than wild-type heads[a]

Gender	Age (wk)	Genotype	No. of mice/no. in group		
			No trabecular bone	Partial trabeculation	Complete trabeculation
Female	9	Wild type	7/7	0/7	0/7
		Null	4/9	5/9	0/9
	15	Wild type	7/7	0/7	0/7
		Null	1/7	4/7	2/7
Male	9	Wild type	12/12	0/12	0/12
		Null	1/9	7/9	1/9
	15	Wild type	6/6	0/6	0/6
		Null	0/7	0/7	7/7

[a] Values represent the fraction of mice that were scored in each category.

An additional possible explanation for both the increase in cross-sectional area and the alteration in endochondral ossification in long bones of TSP3-null mice is the early increase in body weight of these mice. Kodama et al. (18) have shown an increase in periosteal perimeter, cortical area, and periosteal mineral apposition rate in tibiae from C57BL/6 mice when the

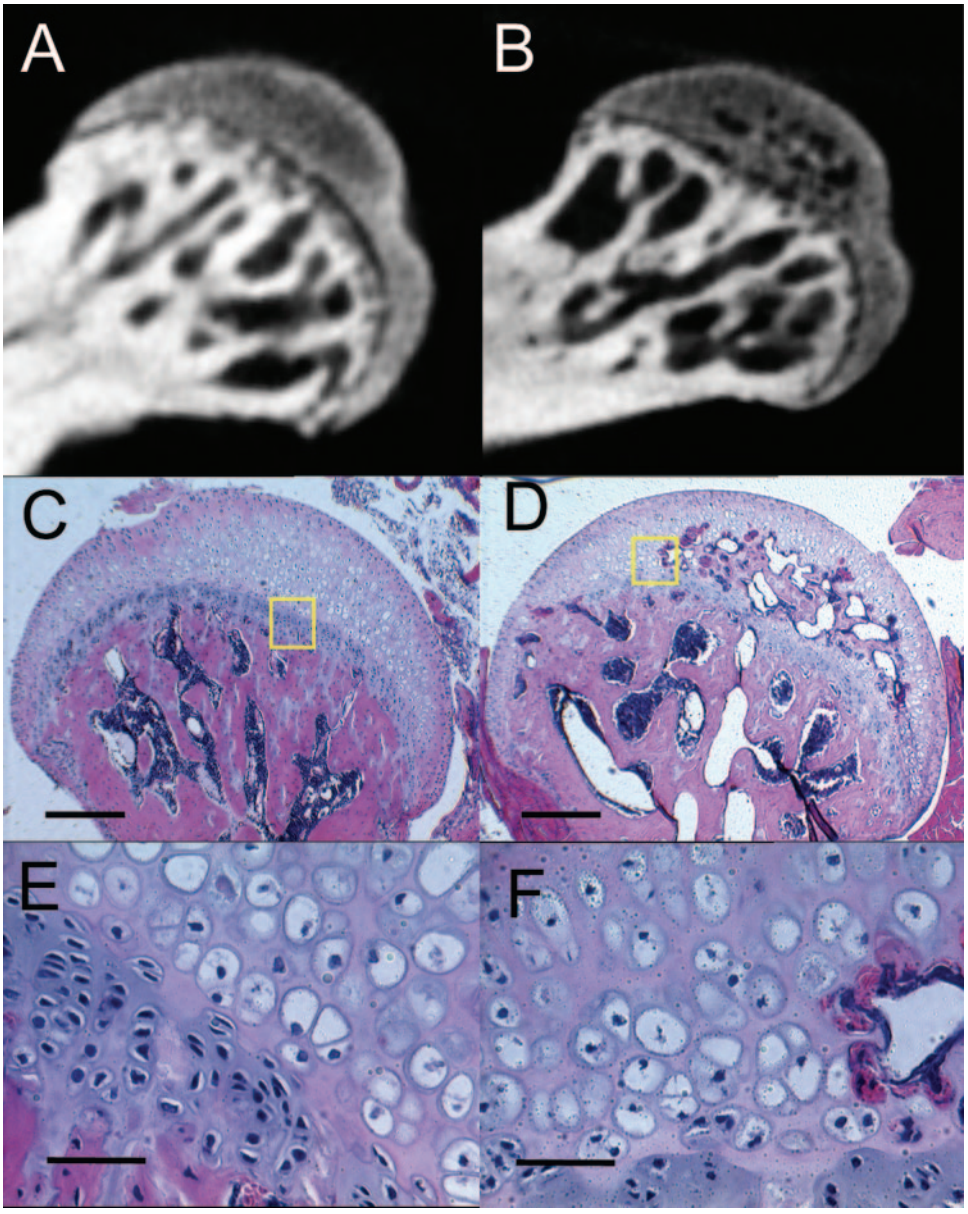

FIG. 3. Gray homogenous area visualized by microCT scans corresponds to hypertrophic chondroctyes. (A, C, and E) Sections from the same femoral head of a 9-week-old wild-type mouse. (B, D, and F) Sections from the femoral head of a 9-week-old TSP3-null mouse. (A and B) MicroCT images of the femoral head. (C to F) Sections stained with hematoxylin and eosin. (E and F) Higher-magnification images of panels C and D, respectively, corresponding to the areas indicated by the yellow boxes. In panels C and E (WT), note that the entire femoral head, proximal to the growth plate is composed of hypertrophic chondrocytes, whereas in panels D and F (TSP3-null) the proximal femoral head is partially ossified and composed of areas of trabecular bone. Some hypertrophic chondrocytes remain. Measurement bars in panels C and D represent 250 μm, and those in panels E and F represent 50 μm.

animals were subjected to higher mechanical loads. Mechanical factors may also contribute to ossification of femoral head cartilage. Thus, the formation of trabecular bone reinforces long bones that are subjected to increased loading resulting from increased body weight (13) and an increase in shear stress is linked to the transformation of cartilage into trabecular bone (3). Similarly, the early increase in body weight of TSP3-null mice may cause an increase in shear stress and thereby accelerate the formation of trabecular bone.

Although increased body weight may contribute to the skeletal phenotype, we believe it is unlikely to represent the sole cause. Appreciable differences in bone geometry and in femoral head ossification persist in 15-week males, despite the absence of statistically significant differences in body weight. Given the presence of TSP3 in cartilage and bone, we postulate that TSP3 is playing a role locally in regulating postnatal bone modeling and endochondral ossification. In view of the broad distribution of TSP3 during development, it is likely that other abnormalities will be found as these mice are studied further, and such new findings could help to determine whether in-

creased body mass is a primary or secondary factor in establishing the phenotype of TSP3-null mice. In particular we anticipate that as we examine secondary centers that ossify much earlier than the femoral head, we will see a similar pattern of accelerated ossification in TSP3-null mice.

The mechanism by which TSP3 might regulate bone maturation and ossification of calcified cartilage is presently unknown. Guo et al. (14) have shown that retinoic acid and vitamin D_3 can bind to the axial pore in TSP5. Both of these factors play a role in endochondral ossification, so a disruption of a similar interaction with TSP3 is a possible cause of the phenotypic abnormalities in TSP3-null mice. Another basis for the changes in bone in TSP3-null mice is the possible interaction of TSP3 with type IX collagen. Type IX collagen is present in cartilage (11) and is known to interact with the C terminus of TSP5 (16). Alterations in this interaction have been implicated as possible causes of pseudoachondroplasia and multiple epiphyseal dysplasia (16, 27). Alternatively, TSP3 could function by interacting with various cell types during the process of ossification, or the protein could play a direct structural role.

Since TSP3 appears to be required for proper progression of postnatal endochondral ossification, it is surprising that its absence does not have an impact on prenatal skeletal patterning, as judged by Alcian blue/Alizarin red S staining. Iruela-Arispe et al. have previously used in situ hybridization to show that TSP3 is present in murine fetal cartilage as early as 15 days postconception (17). Similarly, Svensson et al. did not report any phenotypic alterations in COMP/TSP5-deficient mice, despite the prevalence of COMP in growth cartilage (26). When one considers the homology in structure and the overlapping expression patterns between TSP3 and COMP, it is possible that COMP and TSP3 play compensatory roles in reducing the severity of the phenotypes of TSP3-null and COMP-null mice, respectively. However, we do not think that overlapping functions explain the mild phenotypes of TSP3-null and COMP-null mice. We have generated double TSP3/TSP5 knockout mice, and preliminary analysis has not revealed an increase in severity of the phenotype in these mice. For example, both TSP3-null and double knockout mice show similar increases in bone geometric and mechanical properties relative to wild-type mice (K. Hankenson and P. Bornstein, unpublished results).

In conclusion, this study demonstrates that TSP3 regulates postnatal skeletal maturation. At 9 weeks, TSP3-null femurs show an increase in mid-cortical moment of inertia which in turn results in enhanced bending strength of the bones. Most significantly, TSP3 affects the rate of endochondral ossification. Thus, in the absence of TSP3, there is accelerated ossification of femoral head calcified cartilage.

ACKNOWLEDGMENTS

This study was supported by grants HL 18645 and AR45418 from the National Institutes of Health to P.B., grant AR8562 to K.D.H., the University of Michigan Bone Center (AR46024), and a Postdoctoral Fellowship from the Arthritis Foundation awarded to S.H.

We thank Carol Ware and the Nathan Shock Center for Aging for assistance with blastocyst injections and generation of chimeric mice, Bernard Buetow for expertise in mouse histopathology, Janet Hall for expertise in statistical analysis, and Jennifer Tullis, Emily Stainbrook, Ken Kozloff, Suzanne Volkman, David Fischer, Rochelle Taylor, John Baker, and Daniel Meram for skillful technical assistance.

REFERENCES

1. **Adams, J. C.** 2001. Thrombospondins: multifunctional regulators of cell interactions. Annu. Rev. Cell Dev. Biol. **17:**25–51.
2. **Adolph, K. W.** 1999. Relative abundance of thrombospondin 2 and thrombospondin 3 mRNAs in human tissues. Biochem. Biophys. Res. Commun. **258:**792–796.
3. **Beaupre, G. S., S. S. Stevens, and D. R. Carter.** 2000. Mechanobiology in the development, maintenance, and degeneration of articular cartilage. J. Rehabil. Res. Dev. **37:**145–151.
4. **Bornstein, P., S. Devarayalu, S. Edelhoff, and C. M. Disteche.** 1993. Isolation and characterization of the mouse thrombospondin 3 (Thbs3) gene. Genomics **15:**607–613.
5. **Bornstein, P., C. E. McKinney, M. E. LaMarca, S. Winfield, T. Shingu, S. Devarayalu, H. L. Vos, and E. I. Ginns.** 1995. Metaxin, a gene contiguous to both thrombospondin 3 and glucocerebrosidase, is required for embryonic development in the mouse: implications for Gaucher disease. Proc. Natl. Acad. Sci. USA **92:**4547–4551.
6. **Bornstein, P., and E. H. Sage.** 1994. Thrombospondins. Methods Enzymol. **245:**62–85.
7. **Brodt, M. D., C. B. Ellis, and M. J. Silva.** 1999. Growing C57BL/6 mice increase whole bone mechanical properties by increasing geometric and material properties. J. Bone Miner. Res. **14:**2159–2166.
8. **Chomczynski, P., and N. Sacchi.** 1987. Single-step method of RNA isolation by acid guanidinium thiocyanate-phenol-chloroform extraction. Anal. Biochem. **162:**156–159.
9. **Collins, M., and P. Bornstein.** 1996. SP1-binding elements, within the common metaxin-thrombospondin 3 intergenic region, participate in the regulation of the metaxin gene. Nucleic Acids Res. **24:**3661–3669.
10. **Collins, M., P. Rojnuckarin, Y. H. Zhu, and P. Bornstein.** 1998. A far upstream, cell type-specific enhancer of the mouse thrombospondin 3 gene is located within intron 6 of the adjacent metaxin gene. J. Biol. Chem. **273:**21816–21824.
11. **Cremer, M. A., E. F. Rosloniec, and A. H. Kang.** 1998. The cartilage collagens: a review of their structure, organization, and role in the pathogenesis of experimental arthritis in animals and in human rheumatic disease. J. Mol. Med. **76:**275–288.
12. **Engel, J.** 2004. Role of oligomerization domains in thrombospondins and other extracellular matrix proteins. Int. J. Biochem. Cell Biol. **36:**997–1004.
13. **Felisbino, S. L., and H. F. Carvalho.** 2001. Growth cartilage calcification and formation of bone trabeculae are late and dissociated events in the endochondral ossification of Rana catesbeiana. Cell Tissue Res. **306:**319–323.
14. **Guo, Y., D. Bozic, V. N. Malashkevich, R. A. Kammerer, T. Schulthess, and J. Engel.** 1998. All-trans retinol, vitamin D and other hydrophobic compounds bind in the axial pore of the five-stranded coiled-coil domain of cartilage oligomeric matrix protein. EMBO J. **17:**5265–5272.
15. **Hankenson, K. D., S. D. Bain, T. R. Kyriakides, E. A. Smith, S. A. Goldstein, and P. Bornstein.** 2000. Increased marrow-derived osteoprogenitor cells and endosteal bone formation in mice lacking thrombospondin 2. J. Bone Miner. Res. **15:**851–862.
16. **Holden, P., R. S. Meadows, K. L. Chapman, M. E. Grant, K. E. Kadler, and M. D. Briggs.** 2001. Cartilage oligomeric matrix protein interacts with type IX collagen, and disruptions to these interactions identify a pathogenetic mechanism in a bone dysplasia family. J. Biol. Chem. **276:**6046–6055.
17. **Iruela-Arispe, M. L., D. J. Liska, E. H. Sage, and P. Bornstein.** 1993. Differential expression of thrombospondin 1, 2, and 3 during murine development. Dev. Dyn. **197:**40–56.
18. **Kodama, Y., Y. Umemura, S. Nagasawa, W. G. Beamer, L. R. Donahue, C. R. Rosen, D. J. Baylink, and J. R. Farley.** 2000. Exercise and mechanical loading increase periosteal bone formation and whole bone strength in C57BL/6J mice but not in C3H/Hej mice. Calcif. Tissue Int. **66:**298–306.
19. **Kuhn, J. L., S. A. Goldstein, L. A. Feldkamp, R. W. Goulet, and G. Jesion.** 1990. Evaluation of a microcomputed tomography system to study trabecular bone structure. J. Orthop. Res. **8:**833–842.
20. **Laird, P. W., A. Zijderveld, K. Linders, M. A. Rudnicki, R. Jaenisch, and A. Berns.** 1991. Simplified mammalian DNA isolation procedure. Nucleic Acids Res. **19:**4293.
21. **Liu, X., H. Wu, J. Loring, S. Hormuzdi, C. M. Disteche, P. Bornstein, and R. Jaenisch.** 1997. Trisomy eight in ES cells is a common potential problem in gene targeting and interferes with germ line transmission. Dev. Dyn. **209:**85–91.
22. **Malashkevich, V. N., R. A. Kammerer, V. P. Efimov, T. Schulthess, and J. Engel.** 1996. The crystal structure of a five-stranded coiled coil in COMP: a prototype ion channel? Science **274:**761–765.
23. **Ozbek, S., J. Engel, and J. Stetefeld.** 2002. Storage function of cartilage oligomeric matrix protein: the crystal structure of the coiled-coil domain in complex with vitamin D(3). EMBO J. **21:**5960–5968.
24. **Qabar, A., L. Derick, J. Lawler, and V. Dixit.** 1995. Thrombospondin 3 is a pentameric molecule held together by interchain disulfide linkage involving two cysteine residues. J. Biol. Chem. **270:**12725–12729.
25. **Qabar, A. N., Z. Lin, F. W. Wolf, K. S. O'Shea, J. Lawler, and V. M. Dixit.**

1994. Thrombospondin 3 is a developmentally regulated heparin binding protein. J. Biol. Chem. **269:**1262–1269.
26. **Svensson, L., A. Aszodi, D. Heinegard, E. B. Hunziker, F. P. Reinholt, R. Fassler, and A. Oldberg.** 2002. Cartilage oligomeric matrix protein-deficient mice have normal skeletal development. Mol. Cell. Biol. **22:**4366–4371.
27. **Thur, J., K. Rosenberg, D. P. Nitsche, T. Pihlajamaa, L. Ala-Kokko, D. Heinegard, M. Paulsson, and P. Maurer.** 2001. Mutations in cartilage oligomeric matrix protein causing pseudoachondroplasia and multiple epiphyseal dysplasia affect binding of calcium and collagen I, II, and IX. J. Biol. Chem. **276:**6083–6092.
28. **Tucker, R. P., C. Hagios, R. Chiquet-Ehrismann, and J. Lawler.** 1997. In situ localization of thrombospondin-1 and thrombospondin-3 transcripts in the avian embryo. Dev. Dyn. **208:**326–337.
29. **Turner, C. H., Y. F. Hsieh, R. Muller, M. L. Bouxsein, D. J. Baylink, C. J. Rosen, M. D. Grynpas, L. R. Donahue, and W. G. Beamer.** 2000. Genetic regulation of cortical and trabecular bone strength and microstructure in inbred strains of mice. J. Bone Miner. Res. **15:**1126–1131.
30. **Urry, L. A., C. A. Whittaker, M. Duquette, J. Lawler, and D. W. DeSimone.** 1998. Thrombospondins in early Xenopus embryos: dynamic patterns of expression suggest diverse roles in nervous system, notochord, and muscle development. Dev. Dyn. **211:**390–407.
31. **Vos, H. L., S. Devarayalu, Y. de Vries, and P. Bornstein.** 1992. Thrombospondin 3 (Thbs3), a new member of the thrombospondin gene family. J. Biol. Chem. **267:**12192–12196.
32. **Vos, H. L., M. Mockensturm-Wilson, P. M. Rood, A. M. Maas, T. Duhig, S. J. Gendler, and P. Bornstein.** 1995. A tightly organized, conserved gene cluster on mouse chromosome 3 (E3–F1). Mamm. Genome **6:**820–822.